analytical chemistry

pubs.acs.org/ac

Article

Smartphone-Based Electrochemical Immunoassay for Point-of-Care Detection of SARS-CoV-2 Nucleocapsid Protein

Ruijin Zeng, Minghao Qiu, Qing Wan, Zhisheng Huang, Xiaolong Liu, Dianping Tang,* and Dietmar Knopp*

Cite This: https://doi.org/10.1021/acs.analchem.2c03606

Read Online

ACCESS | Metrics & More | Article Recommendations | Supporting Information

ABSTRACT: Large-scale, rapid, and inexpensive serological diagnoses of severe acute respiratory syndrome-coronavirus-2 (SARS-CoV-2) are of great interest in reducing virus transmission at the population level; however, their development is greatly plagued by the lack of available point-of-care methods, leading to low detection efficiency. Herein, an ultrasensitive smartphone-based electrochemical immunoassay is reported for rapid (less than 5 min), low-cost, easy-to-implement detection of the SARS-CoV-2 nucleocapsid protein (SARS-CoV-2 N protein). Specifically, the electrochemical immunoassay was fabricated on a screen-printed carbon electrode coated with electrodeposited gold nanoparticles, followed by incubation of anti-N antibody (Ab) and bovine serum albumin as the working electrode. Accompanied by the antigen−antibody reaction between the SARS-CoV-2 N protein and the Ab, the electron transfer between the electroactive species $[Fe(CN)_6]^{3-}/^{4-}$ and the electrode surface is disturbed, resulting in reduced square-wave voltammetry currents at 0.075 V versus the Ag/AgCl reference electrode. The proposed immunoassay provided a good linear range with SARS-CoV-2 N protein concentrations within the scope of 0.01−1000 ng/mL (R^2 = 0.9992) and the limit of detection down to 2.6 pg/mL. Moreover, the detection data are wirelessly transmitted to the interface of the smartphone, and the corresponding SARS-CoV-2 N protein concentration value is calculated and displayed. Therefore, the proposed portable detection mode offers great potential for self-differential diagnosis of residents, which will greatly facilitate the effective control and large-scale screening of virus transmission in resource-limited areas.

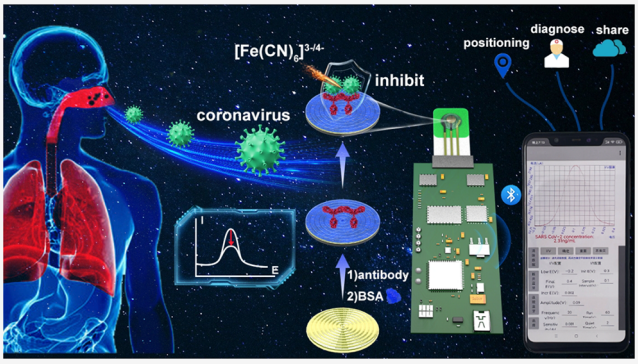

The emergence of the fatal, ever-persistent severe acute respiratory syndrome coronavirus 2 (SARS-CoV-2) has been regarded as a ravage of the public healthcare system; it is the extremely contagious pathogen of acute pneumonia COVID-19.[1−3] According to the World Health Organization's weekly epidemiological update, as of 7 August 2022, around 6.4 million death cases have been reported globally, further causing continued damage to public confidence in the treatment and the economy. Among the different assays considered to have played an extraordinary role in disease screening, polymerase chain reaction (PCR) has become the most widely used due to the sequence specificity and high sensitivity of the nucleic acid. However, PCR not only suffers from the risk of secondary infection caused by on-site screening and aggregation but also requires trained laboratory personnel to perform detection using complex and expensive equipment, which limits the application of PCR-based large-scale screening in resource-limited areas.[4−7] Alternatively, the point-of-care (POC) testing represented by the lateral flow assay (LFA) is an important means of home self-checking, which can achieve diagnosis while avoiding cluster infection caused by PCR sampling.[8] Despite the widespread use of SARS-CoV-2-based LFAs, questions remain about their accuracy, such as false-negative results for trace antibodies following nonprofessional manipulations, rendering the test ineffective. In addition, different people's sensitivity to color will lead to different quantitative results for the same experimental results. In this regard, exploring a highly sensitive, less-required, results-visualized, and accurately quantifiable diagnosis is of great significance for POC detection of SARS-CoV-2.[9]

The ingenious combination of the extremely low detection limit of electrochemical immunodetection and the highly integrated electronic device gets rid of the traditional electrochemical workstation, which is a new trend for the application of electrochemical sensing toward POC applications.[10−12] Recently, diverse electrochemical schemes involving smartphones have been reported in the detection of SARS-

Received: August 17, 2022
Accepted: October 7, 2022

Scheme 1. Schematic Illustration of POC Electrochemical Immunoassay for Detection of SARS-CoV-2 N Protein with Smartphone Visual Readout

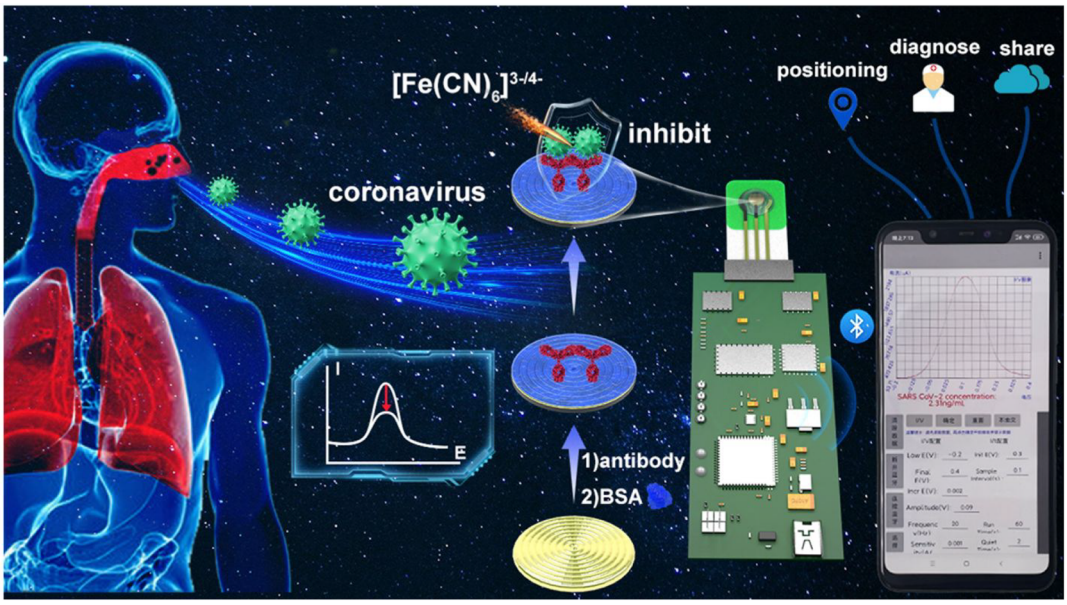

CoV-2 because of portability and ease of operation.[13] For instance, Li et al. proposed a microfluidic immunosensor for rapid, highly sensitive, and portable measurement of the nucleocapsid protein of SARS-CoV-2 (SARS-CoV-2 N protein) in serum using a hand-held diagnostic device.[14] Torres et al. reported that a specific molecular recognition event between the SARS-CoV-2 spike protein and angiotensin-converting enzyme-2 was converted into a resistive signal, enabling the detection process on a smartphone.[15] Although some works have demonstrated that the electrochemical detection process signal can be read on a smartphone, further improvements such as direct calculation of the corresponding current and calculation of the equivalent concentration of SARS-CoV-2 have not been reported.[16,17]

In the present study, we demonstrate an electrochemical immunoassay for POC detection of the SARS-CoV-2 N protein with a smartphone visual readout (Scheme 1). The proposed immunoassay was constructed with gold nanoparticles (AuNPs) electrodeposited on a screen-printed carbon electrode (SPCE) and allowed covalent binding between the anti-N antibody (Ab) and AuNPs/SPCE during incubation. Afterward, the bovine serum albumin (BSA) was coated on the Ab/AuNPs/SPCE to block the unbonded sites. When Ab specifically binds to the SARS-CoV-2 N protein, the electron transfer between the electroactive probe $[Fe(CN)_6]^{3-/4-}$ and the electrode surface is disturbed, thereby reducing the peak current of the square-wave voltammetry (SWV) technique. To further visualize the diagnostic results, we combine the electrode testing process with a highly integrated circuit, so that the current is displayed on the smartphone during the testing process. The relevant algorithm can read the current value and calculate the corresponding SARS-CoV-2 N protein concentration on the smartphone screen through a linear equation. Impressively, the smartphone-based electrochemical immunoassay exhibited high stability after 12 times washing, completing detection within 5 min, with diagnostic results comparable to commercial LFA test strips. We expect that the proposed method can play a significant role in mass screening for SARS-CoV-2 as a common home self-test method.

EXPERIMENTAL SECTION

Materials and Reagents. Sodium phosphate dibasic dodecahydrate ($Na_2HPO_4{\cdot}12H_2O$, AR, 99%), sodium phosphate dibasic dihydrate ($Na_2HPO_4{\cdot}2H_2O$, meets USP testing specifications), potassium chloride (KCl, AR, 99.5%), and gold chloride trihydrate ($HAuCl_4{\cdot}3H_2O$, ≥99.9% trace metals basis) were obtained from Aladdin Biochemical Technology Co., Ltd. (Shanghai, China). Sulfuric acid (H_2SO_4, 95%−98%) was obtained from Sinopharm Chemical Reagent Co., Ltd. (Shanghai, China). Potassium ferricyanide ($K_3Fe(CN)_6$) and potassium ferrocyanide trihydrate ($K_4Fe(CN)_6{\cdot}3H_2O$) were obtained from Fuchen Chemical Reagent Co., Ltd. (Tianjin, China). Bovine serum albumin (BSA) standard solution (0.5 mg/mL), alpha-fetoprotein antigen (AFP), carcinoembryonic antigen (CEA), and prostate specific antigen (PSA) were obtained from Wuhan Cusabio Biotech. Inc. (Wuhan, China, https://www.cusabio.com/). LFA (http://en.hotgen.com.cn/), SARS-CoV-2 nucleocapsid (N) protein (http://www.cell-regen.com/productshow_167.html), anti-N antibody (http://www.ebiocore.com/), influenza A (Flu A), and influenza B (Flu B) were kindly provided by Mengchao Hepatobiliary Hospital of Fujian Medical University (Fuzhou, China). All protein solutions, including BSA, antigens, and antibodies, were prepared in PBS (10 mM, pH 7.4).

The electrochemical measurements were performed by CHI 660E from Chenhua Instrument Co., Ltd. (Shanghai, China). The screen-printed carbon electrode (SPCE, 3.4 cm × 1.2 cm) was purchased from Taobao (http://chinstr.com/). Deionized water was obtained from a Millipore water purification system (18.2 MΩ·cm, Milli-Q, Germany).

Preparation of Immunoassay on SPCE and Electrochemical Detection. The modification of AuNPs on SPCE was achieved by electrodeposition. Specifically, a mixture of chloroauric acid (100 μL, 2 M, containing 0.5 M of H_2SO_4) was dropped on the entire surface of SPCE, and the electrodeposit step was performed by cyclic voltammetry (CV) technology, starting from −0.2 to −1.4 V for 10 segments CV scans with a sensitivity of 10^{-2} and a scan rate of

https://doi.org/10.1021/acs.analchem.2c03606
Anal. Chem. XXXX, XXX, XXX−XXX

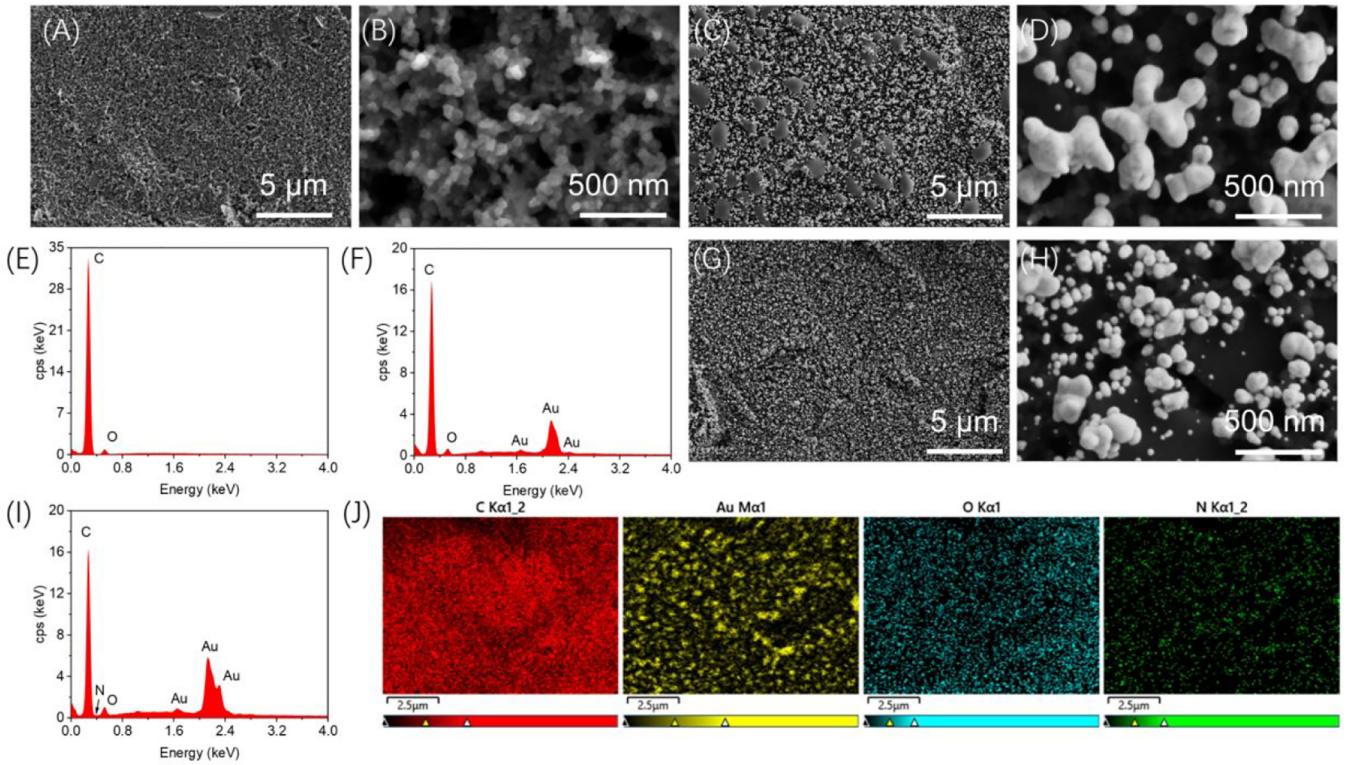

Figure 1. SEM image of (A, B) SPCE and (C, D) AuNPs/SPCE. EDS of (E) SPCE and (F) AuNPs/SPCE. (G, H) SEM images, (I) EDS, and (J) element mapping of BSA/Ab/AuNPs/SPCE.

50 mV/s, followed by gentle washing of the electrode surface three times with PBS (10 mM, 100 μL, pH 7.4). Then, without touching the electrode surface, the liquid on the electrode was carefully blotted with filter paper, and the pale yellow-brown AuNPs-modified working electrode could be observed (AuNPs/SPCE). Subsequently, an Ab solution (10 μg/mL, 10 μL) was incubated on the working electrode for 30 min using the drop-casting method. Then, the same washing steps were performed to remove Ab that was not bound to the AuNPs (Ab/AuNPs/SPCE). Thereafter, the blocking agent BSA (0.5%, 10 μL) was lightly covered on the working electrode and incubated for 45 min to avoid the nonspecific binding of the sample in the subsequent test to the electrode. Finally, the fabricated BSA/Ab/AuNPs/SPCE electrode is connected to the designed integrated circuit for further use. For SWV detection, PBS (10 mM, 100 μL, pH 7.4) containing different concentrations of SARS-CoV-2 N protein was incubated on the BSA/Ab/AuNPs/SPCE surface for 4.5 min. The mixture of $[Fe(CN)_6]^{3-/4-}$ (10 mM, 100 μL, containing 0.1 M KCl) was dropped after washing with PBS (10 mM, 100 μL, pH 7.4). Then, the immunosensor was connected to the smartphone/electrochemical workstation for SWV detection (scanning from −0.2 to 0.4 V; frequency, 20 Hz; amplitude, 90 mV; sensitivity, 10^{-3}).

LFA-Based Detection. The sample (5 μL with different concentration) was dissolved in a commercial extraction solution (200 μL; main components are PBS, NaCl, and Tween-20), and then, a pipet was used to add the sample (100 μL) to the sample hole (S) of the detection card. After standing at room temperature for 15 min, the results of the C-line and T-line were observed.

RESULTS AND DISCUSSION

Morphological Characterization of SPCE. As mentioned before, the modification of the electrode surface is the key to the construction of a highly sensitive electrochemical immunosensor toward SARS-CoV-2 N protein detection. The CV profiles of electrodeposited AuNPs on SPCE are shown in Figure S1. In the case of a CV negative sweep, the reduction current increases sharply at −0.65 V, which may be mainly due to the progress of the deposition of AuNPs and the hydrogen evolution reaction. At the same time, the response current remains the same as before after the positive sweep. The morphologies before and after electrodeposition of AuNPs on the surfaces of SPCE electrodes were characterized by scanning electron microscopy (ZEISS Gemini 300). As shown in Figure 1A and B, the bare SPCE electrode surface contains graphite flakes of different sizes and a high content of aggregated carbon particles. After electrodepositing AuNPs on the surface of SPCE, it can be observed that many AuNPs or aggregated large particles are distributed on the surface of AuNPs/SPCE (Figure 1C, D). The energy dispersive spectrometer (EDS, Figure 1E, F) analysis before and after electrodeposition showed that the presence of the Au element after electrodeposition corresponds to the presence of AuNPs. Furthermore, there was no obvious change after AuNPs/SPCE surface modification with Ab and BSA via $-NH_2$ groups with Au interaction (Figure 1G, H).[18,19] The corresponding EDS and elemental mapping (Figure 1I, J; Figure S2) proved the existence of C, Au, N, and O elements on the electrode surface. The presence of the N element indicated the presence of protein on the electrode surface, but further electrochemical characterization is required to demonstrate the stepwise modification process due to the low content of the N element.

https://doi.org/10.1021/acs.analchem.2c03606
Anal. Chem. XXXX, XXX, XXX−XXX

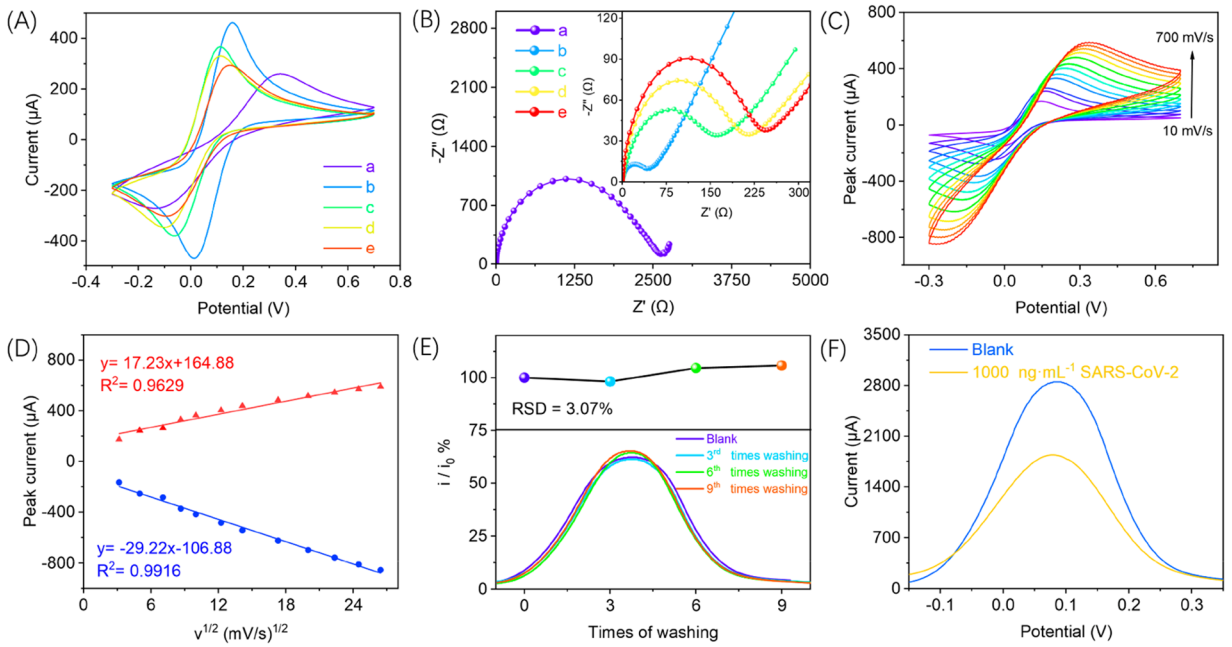

Figure 2. (A) CV and (B) EIS measured in different processes: (a) SPCE, (b) AuNPs/SPCE, (c) Ab/AuNPs/SPCE, (d) BSA/Ab/AuNPs/SPCE, and (e) SARS-CoV-2 N protein/BSA/Ab/AuNPs/SPCE. (C) CV plot and (D) corresponding regression equations between the anodic/cathodic peak currents versus scan rate $v^{1/2}$ ranging from 10, 25, 50, 75, 100, 150, 200, 300, 400, 500, 600, and 700 mV/s. (E) Stability of SARS-CoV-2 N protein/BSA/Ab/AuNPs/SPCE after three, six, and nine times washing. (F) Feasibility evaluation of the proposed immunoassay measured by adding 1000 ng/mL SARS-CoV-2 N protein.

Electrochemical Performance of Modification Process. To verify the electrochemical performance of each modification process, CV and electrochemical impedance spectroscopy (EIS) were utilized for corresponding electrodes. For the CV technique, the reversibility of the electrode for the redox reaction could be determined by the peak current of $[Fe(CN)_6]^{4-/3-}$ and the corresponding potential difference ΔE (Figure 2A). The bare SPCE possessed the smallest peak current (262.3 μA) on the electrode surface and the largest ΔE (0.477 V), indicating that the most difficult reversible redox reaction occurred at this electrode (curve a). Moreover, the reversibility of the redox reaction on the AuNPs/SPCE electrode surface was enhanced by electrodeposition of AuNPs due to the good electrical conductivity of AuNPs, which matched the experimental phenomenon of the greatly increased peak current (466.6 μA) and greatly reduced ΔE (0.144 V) (curve b). Besides, with the incubation of Ab, the peak current (370.4 μA) decreased on the Ab/AuNPs/SPCE electrode surface, and ΔE (0.172 V) further increased, which may be attributed to the hydrophobic interaction and steric hindrance of Ab hindering the electron diffusion process (curve c). Similarly, the peak current (331.9 μA and 296.0 μA) and ΔE (0.212 and 0.244 V) continued to decrease and increase, respectively, when the electrode surface was further incubated with BSA (curve d) and SARS-CoV-2 N protein (curve e).

To further match the conclusions of the CV results, we also subjected the above electrodes to EIS testing. In general, the diameter of the semicircular Nyquist plot represents the electron-transfer resistance (R_{ct}). As shown in Figure 2B, the R_{ct} value (curve b, ~42.2 Ω) of the AuNPs/SPCE electrode surface decreased relative to that of SPCE after electrodeposition of AuNPs (curve a, ~2620 Ω), attributed to the excellent electrical conductivity of AuNPs. Subsequently, with the incubation of Ab (curve c, ~163 Ω), BSA (curve d, ~211 Ω), and antigen (curve e, ~247 Ω), the R_{ct} value continuously increased due to the hydrophobic interaction and steric hindrance of protein molecules, resulting in a decrease in the efficiency of electron participation in redox reactions. The EIS and CV results are consistent, both confirming the success of the stepwise modification of the electrode surface.

Finally, a series of CV scans were performed on SARS-CoV-2 N protein/BSA/Ab/AuNPs/SPCE with scan rates ranging from 10 to 700 mV/s to further understand the mechanism of $[Fe(CN)_6]^{4-/3-}$ in electrochemical detection. As described in Figure 2C and D, the peak current (including the anodic/cathodic peak current) had good linearity with the square root of the scan rate, demonstrating the diffusion-control behavior of $[Fe(CN)_6]^{4-/3-}$ in the redox reaction.[20]

Stability and Feasibility of Electrochemical Immunoassay. Although the above experimental results show the successful assembly of the electrodes, it is important to evaluate the stability to ensure that no false positives will occur due to washing. As described in Figure 2E, the SWV peak shape and peak current remained essentially unchanged after washing the electrode surface with PBS (10 mM, 100 μL, pH 7.4) for the three, six, and nine times. An acceptable variation in peak current can be observed (relative standard deviation, RSD = 3.07%), indicating satisfactory stability of the constructed BSA/Ab/AuNPs/SPCE electrode. Figure 2F shows that the peak current of SWV was significantly reduced when BSA/Ab/AuNPs/SPCE was incubated with a SARS-CoV-2 N protein solution (1000 ng/mL, 4.5 min). When the sensor recognizes the presence of the N protein, the corresponding redox reaction efficiency of $[Fe(CN)_6]^{4-/3-}$ decreases, resulting in a decrease in the SWV peak current due to the formation of antigen−antibody complexes and steric hindrance effects. Therefore, the proposed electrochemical

https://doi.org/10.1021/acs.analchem.2c03606
Anal. Chem. XXXX, XXX, XXX−XXX

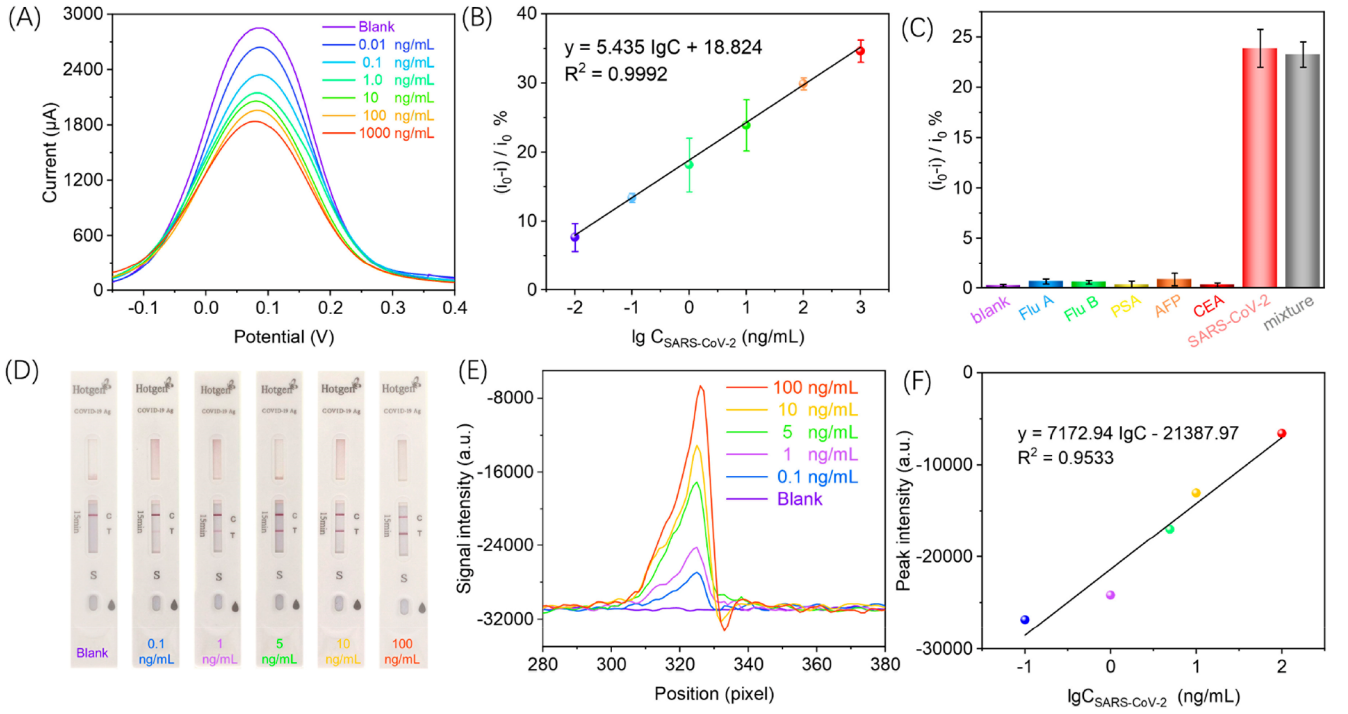

Figure 3. (A) SWV current of electrochemical immunoassay toward SARS-CoV-2 N protein. (B) Calibration plots between $(i_0 - i)/i_0$% and the logarithm of the SARS-CoV-2 N protein concentration ranging from 0.01, 0.1, 1.0, 10, 100, and 1000 ng/mL. (C) Selectivity against Flu A, Flu B, PSA, AFP, CEA, SARS-CoV-2 N protein, and the mixtures containing the aforementioned analytes. (D) Photographs of LFA test cards after reaction with SARS-CoV-2 N protein concentrations of 0, 0.1, 1, 5, 10, and 100 ng/mL. (E) Corresponding signal intensity of the grayscale of the T-line color. (F) Linear relationship between peak signal intensity and SARS-CoV-2 N protein concentration.

Table 1. Comparison of Different Assay Methods for SARS-CoV-2 N Protein Determination with Analytical Properties

Methods	Linear range (ng/mL)	LOD (pg/mL)	Detection time	Instrument/DDC[a]	ref
Microfluidic magneto immunosensor	0−10	50/10	~85 min	potentiostat and smartphone/no	14
Serological aptamer-assisted proximity ligation assay	0.05−5	30.9/37.5	~120 min	PCR machine/no	21
BioFET[b]-based immunoassays	0.4−400	340/140	within 30 min	FET or smartphone/no	22
EIS immunoassays	0.1−10	100	75 min	ToAD[c] system/no	23
Plasmonic immunoassays	150−550	1.5×10^5	5 min	UV−visible spectrometry/no	24
Immunochromatographic sensor	0.05−1.6	25	25 min	smartphone/no	25
Smartphone-based immunoassays	0.01−1000	2.6	5 min	smartphone/yes	This work

[a]DDC: directly display the concentration. [b]BioFET: field-effect transistor-based biosensing. [c]ToAD: multichannel impedance analyzer with a 96-interdigitated microelectrode sensor.

immunoassay can be used to quantitatively monitor the concentration of the SARS-CoV-2 N protein.

Analytical Performance of Electrochemical Immunoassay. A series of SARS-CoV-2 N protein concentrations (0, 0.01, 0.1, 1, 10, 100, 1000 ng/mL) in PBS were incubated on the BSA/Ab/AuNPs/SPCE for 4.5 min to obtain the calibration curve. As described in Figure 3A, the peak current of SWV decreased accordingly with an increased concentration of the SARS-CoV-2 N protein. Preferable linear-dependence relative current change (the percentage decrease in the peak current; $i_0 - i/i_0$%; i and i_0 represent the SWV peak current with and without analyte, respectively) concentration curves were acquired, and the corresponding regression equation was $i_0 - i/i_0\% = 18.824 + 5.435 \times \lg C_{[\text{SARS-CoV-2}]}$ (ng/mL, R^2 = 0.9903, n = 7) with a limit of detection (LOD) of 2.6 pg/mL (S/N = 3) (Figure 3B). More importantly, compared with other strategies to detect the SARS-CoV-2 N protein (Table 1), this work enables lower LOD and more portable detection technology and readout. Besides, the maximum RSDs were 6.31% for intra-assays and 9.79% for interassays toward 0.1, 10, and 100 ng/mL of SARS-CoV-2 N protein, respectively, indicating good reproducibility. The selectivity of the electrochemical immunoassay was then examined using other biomarkers or virus antigens as a negative control, including Flu A, Flu B, CEA, AFP, and CEA. In the presence of 10 ng/mL of nontarget protein, the percentage decrease in the peak current of the electrode surface was similar to the blank sample. Furthermore, in the presence of 10 ng/mL of SARS-CoV-2 N protein and nontarget protein, the percentage decreases in the peak current were similar to those in the presence of 10 ng/mL of SARS-CoV-2 N protein alone, indicating no cross-reactivity leading to false-positives/false-negatives (Figure 3C).

Analytical Performance of Commercialized LFA. As a comparison, we further manipulated the commercialized LFA to compare the linear range with the electrochemical

https://doi.org/10.1021/acs.analchem.2c03606
Anal. Chem. XXXX, XXX, XXX−XXX

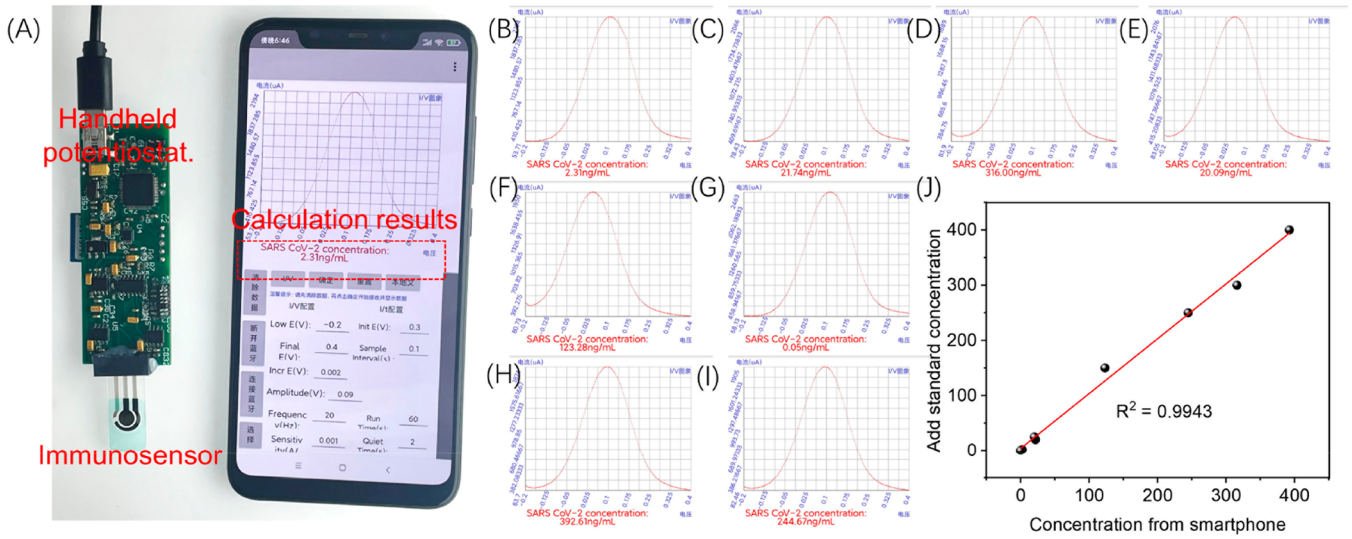

Figure 4. (A) Diagram of the smartphone-based electrochemical immunosensor detection device. (B–I) Smartphone screenshots of SARS-CoV-2 N protein assay results spiked at different concentrations in the mixture. (J) Comparison of spiked and smartphone-calculated concentrations.

immunoassays described above. Typically, LFA-based immunoassays are primarily used for qualitative analysis of the N protein by estimating the colorimetric of control line and test line (C-line and T-line, respectively) by naked eyes. Nonetheless, the detection cards were photographed to measure the grayscale of the T-line (the grayscale is smaller when the N protein is more concentrated; i.e., the color is darker, Figure 3D) for quantitative detection. As illustrated in Figure 3E, the relative response of the grayscale signal intensity was measured from 0.1 to 100 ng/mL at the T-line position. The linear regression equation of the signal intensity versus the logarithmic concentration of SARS-CoV-2 N protein was $y = 7172.94 \times \lg C_{[\text{SARS-CoV-2}]}$ (ng/mL) − 21387.97 ($R^2 = 0.9533$) (Figure 3F). Compared with the detection range of 5 orders of magnitude (0.01–1000 ng/mL) for proposed electrochemical immunoassays, LFA imposes strict requirements on the concentration range of the SARS-CoV-2 N protein with a linear range of 3 orders of magnitude (0.1–100 ng/mL). Notably, the strict requirements of consistency in the evaluation of shades of color limited the quantitative detection of LFA-based immunoassays for screening mild and severe cases, which only relied on the naked eye or cameras with low color bits.

To further demonstrate the potential of the designed electrochemical biosensor in clinical diagnosis, six healthy samples and six patient samples were provided by Mengchao Hepatobiliary Hospital of Fujian Medical University. As shown in Figure S3, the relative current change signals triggered from the patients are much stronger than that of the healthy persons. Statistical analysis can further reflect significant differences between healthy and patient populations, demonstrating the applicability of our method in clinical diagnosis. In addition, the signal could maintain 94.9%, 91.1%, and 89.7% of the initial current after storage for the first, third, and sixth months, respectively, indicating acceptable stability.

SARS-CoV-2 N Protein Detection Using a Smartphone. To improve the portability and sample-to-result intuitiveness of the proposed electrochemical immunosensor, we also developed a hand-held diagnostic device for quantitative measurement of the SARS-CoV-2 N protein in saliva and lysate mixtures. As shown in Figure 4A, this portable test mainly consists of a Xiaomi smartphone and a device equipped with SARS-CoV-2 N protein/BSA/Ab/AuNPs/SPCE electrodes. The integrated device can wirelessly transmit the detected current signal to the smartphone app (Figure S4) and convert the current signal into the SARS-CoV-2 N protein concentration on the screen through an internal algorithm. To verify whether the detection current results of the device are as reliable as those of the CHI660E electrochemical workstation, we tested the same electrodes with two methods. The comparison results are shown in Figure S5, and the current intensities detected by the two methods are comparable. Therefore, the fabricated device can replace the electrochemical workstation for detection of the SARS-CoV-2 N protein. To further demonstrate the intuitiveness of the integrated devices and algorithms for detection results, we performed spike detection in mixtures samples. Figure 4B–I is smartphone screenshots of the current values detected by the manufactured hand-held device and the calculated SARS-CoV-2 N protein concentration. As shown in Figure 4J, the detection value using this device has an excellent linear relationship with the added concentration value, indicating that the hand-held smart device has excellent reliability and instant detection.

CONCLUSIONS

In conclusion, we report a highly sensitive (LOD of 2.6 pg/mL) and portable detection of the SARS-CoV-2 N protein within 5 min by a smartphone-based electrochemical immunoassay platform. Crucially, the fabricated electronic device is comparable to the electrochemical workstation detection results, capable of quantitatively outputting the electrochemical current signal to the app terminal to display the N protein concentration through an internal algorithm. We highlight that the rapid sample-to-answer turnaround of the proposed smart device can satisfy large-scale screening for the SARS-CoV-2 N protein. Meanwhile, our constructed method has a lower LOD, wider detection range, and faster response time compared with commercial LFA qualitative detection. We expect the proposed platform to play a significant role in patient triage and use at

https://doi.org/10.1021/acs.analchem.2c03606
Anal. Chem. XXXX, XXX, XXX−XXX

home for telemedicine care and remote monitoring due to its unparalleled advantages such as ease of use, saliva sample compatibility, and rapid results.

■ ASSOCIATED CONTENT

Supporting Information

The Supporting Information is available free of charge at https://pubs.acs.org/doi/10.1021/acs.analchem.2c03606.

CV plot of electrodeposited AuNPs on SPCE, SEM image and overlay element mapping of BSA/Ab/AuNPs/SPCE, scattered dot plots of SARS-CoV-2 from healthy samples (negative) and patient samples (positive), block diagram of electronic readout circuit and SWV of the device, and CHI660E under different concentrations (PDF)

■ AUTHOR INFORMATION

Corresponding Authors

Dianping Tang − *Key Laboratory of Analytical Science for Food Safety and Biology (MOE and Fujian Province), Department of Chemistry, Fuzhou University, Fuzhou 350108, People's Republic of China*; Phone: +86-591-2286 6125; Email: dianping.tang@fzu.edu.cn; Fax: +86-591-2286 6135

Dietmar Knopp − *Department of Chemistry, Chair for Analytical Chemistry and Water Chemistry, Institute of Hydrochemistry, Technische Universität München, D-85748 Garching, Germany*; orcid.org/0000-0003-4566-9798; Phone: +49-89-289 54500; Email: dietmar.knopp@mytum.de

Authors

Ruijin Zeng − *Key Laboratory of Analytical Science for Food Safety and Biology (MOE and Fujian Province), Department of Chemistry, Fuzhou University, Fuzhou 350108, People's Republic of China*

Minghao Qiu − *Key Laboratory of Analytical Science for Food Safety and Biology (MOE and Fujian Province), Department of Chemistry, Fuzhou University, Fuzhou 350108, People's Republic of China*

Qing Wan − *School of Electronics and Information Engineering, Hubei University of Science and Technology, Xianning 437100, People's Republic of China*

Zhisheng Huang − *School of Electronics and Information Engineering, Hubei University of Science and Technology, Xianning 437100, People's Republic of China*

Xiaolong Liu − *The United Innovation of Mengchao Hepatobiliary Technology Key Laboratory of Fujian Province, Mengchao Hepatobiliary Hospital of Fujian Medical University, Fuzhou 350025, People's Republic of China*

Complete contact information is available at: https://pubs.acs.org/10.1021/acs.analchem.2c03606

Author Contributions

R. Zeng and M. Qiu contributed equally to this work.

Notes

The authors declare no competing financial interest.

■ ACKNOWLEDGMENTS

We gratefully acknowledge the financial supports from the National Natural Science Foundation of China (Grant 21874022 and 21675029).

■ REFERENCES

(1) Lew, T.; Aung, K.; Ow, S.; Amrun, S.; Sutarlie, L.; Ng, L.; Su, X. *ACS Nano* **2021**, *15*, 12286−12297.

(2) Adeel, M.; Asif, K.; Canzonieri, V.; Barai, H.; Rahman, M.; Daniele, S.; Rizzolio, F. *Sens. Actuators B Chem.* **2022**, *359*, 131591.

(3) Rahman, M. *Chemosensors* **2022**, *10*, 287.

(4) Georgiou, P.; Guy, C.; Hasan, M.; Ahmad, A.; Richards, S.; Baker, A.; Thakkar, N.; Walker, M.; Pandey, S.; Anderson, N.; Grammatopoulos, D.; Gibson, M. *ACS Macro Lett.* **2022**, *11*, 317−322.

(5) Seo, G.; Lee, G.; Kim, M.; Baek, S.; Choi, M.; Ku, K.; Lee, C.; Jun, S.; Park, D.; Kim, H.; Kim, S.; Lee, J.; Kim, B.; Park, E.; Kim, S. *ACS Nano* **2020**, *14*, 5135−5142.

(6) Yousefi, H.; Mahmud, A.; Chang, D.; Das, J.; Gomis, S.; Chen, J.; Wang, H.; Been, T.; Yip, L.; Coomes, E.; Li, Z.; Mubareka, S.; McGeer, A.; Christie, N.; Gray-Owen, S.; Cochrane, A.; Rini, J.; Sargent, E.; Kelley, S. *J. Am. Chem. Soc.* **2021**, *143*, 1722−1727.

(7) Ferreira, A.; de Lima, L.; Torres, M.; de Araujo, W.; de la Fuente-Nunez, C. *ACS Nano* **2021**, *15*, 17453−17462.

(8) Ravalin, M.; Roh, H.; Suryawanshi, R.; Kumar, G.; Pak, J.; Ott, M.; Ting, A. *J. Am. Chem. Soc.* **2022**, *144*, 13663−13672.

(9) Kong, D.; Wang, X.; Gu, C.; Guo, M.; Wang, Y.; Ai, Z.; Zhang, S.; Chen, Y.; Liu, W.; Wu, Y.; Dai, C.; Guo, Q.; Qu, D.; Zhu, Z.; Xie, Y.; Liu, Y.; Wei, D. *J. Am. Chem. Soc.* **2021**, *143*, 17004−17014.

(10) Zeng, R.; Gong, H.; Li, Y.; Li, Y.; Lin, W.; Tang, D.; Knopp, D. *Anal. Chem.* **2022**, *94*, 7442−7448.

(11) Zeng, R.; Tao, J.; Tang, D.; Knopp, D.; Shu, J.; Cao, X. *Nano Energy* **2020**, *71*, 104580.

(12) Zeng, R.; Wang, W.; Chen, M.; Wan, Q.; Wang, C.; Knopp, D.; Tang, D. *Nano Energy* **2021**, *82*, 105711.

(13) Nguyen, V.; Nguyen, H.; Bui, K.; Ko, Y.; Park, B.; Seo, T. *Biosens. Bioelectron.* **2022**, *195*, 113632.

(14) Li, J.; Lillehoj, P. *ACS Sens.* **2021**, *6*, 1270−1278.

(15) Torres, M.; de Araujo, W.; de Lima, L.; Ferreira, A.; de la Fuente-Nunez, C. *Matter* **2021**, *4*, 2403−2416.

(16) Yi, L.; Li, J.; Guo, C.; Li, L.; Liu, J. *J. Med. Devices.* **2015**, *9*, No. 044507.

(17) Ainla, A.; Mousavi, M.; Tsaloglou, M.; Redston, J.; Bell, J.; Fernández-Abedul, M.; Whitesides, G. *Anal. Chem.* **2018**, *90*, 6240−6246.

(18) Ansari, S.; Lopa, N.; Parveen, N.; Shaikh, A.; Rahman, M. *Anal. Methods* **2020**, *12*, 5562−5571.

(19) Wu, Q.; Li, N.; Wang, Y.; Xu, Y.; Wu, J.; Jia, G.; Ji, F.; Fang, X.; Chen, F.; Cui, X. *Anal. Chem.* **2020**, *92*, 3354−3360.

(20) Haghayegh, F.; Salahandish, R.; Hassani, M.; Sanati-Nezhad, A. *ACS Appl. Mater. Interfaces* **2022**, *14*, 10844−10855.

(21) Liu, R.; He, L.; Hu, Y.; Luo, Z.; Zhang, J. *Chem. Sci.* **2020**, *11*, 12157−12164.

(22) Chen, P.; Huang, C.; Wu, C.; Chen, P.; Tripathi, A.; Wang, Y. *Sens. Actuators B Chem.* **2022**, *357*, 131415.

(23) Cho, H.; Shim, S.; Cho, W.; Cho, S.; Baek, H.; Lee, S.; Shin, D. *ACS Sens.* **2022**, *7*, 1676−1684.

(24) Behrouzi, K.; Lin, L. *Biosens. Bioelectron.* **2022**, *195*, 113669.

(25) Liang, C.; Liu, B.; Li, J.; Lu, J.; Zhang, E.; Deng, Q.; Zhang, L.; Chen, R.; Fu, Y.; Li, C.; Li, T. *Sens. Actuators B Chem.* **2021**, *349*, 130718.